Cell Reports
Physical Science

CellPress
OPEN ACCESS

Article

Exfoliation of covalent organic frameworks into MnO_2-loaded ultrathin nanosheets as efficient cathode catalysts for Li-CO_2 batteries

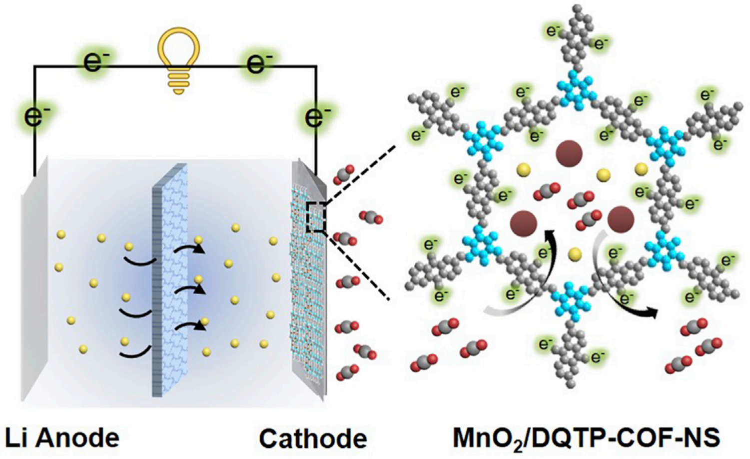

Cheng Jiang, Yu Zhang, Mi Zhang, ..., Yifa Chen, Shun-Li Li, Ya-Qian Lan

chyf927821@163.com (Y.C.)
slli@njnu.edu.cn (S.-L.L.)
yqlan@njnu.edu.cn (Y.-Q.L.)

Highlights

Exfoliation of quinone-based COFs into large-scale and ultrathin nanosheets

MnO_2/DQTP-COF-NS-3 can be applied as high-performance cathode catalyst

DFT study supports the vital role of quinone group in CO_2 reduction reaction

Jiang et al. report exfoliation of quinone-based covalent organic frameworks (COFs) into large-scale and ultrathin MnO_2/DQTP-COF-nanosheet hybrid materials. The ultrathin nanosheets synergistically integrate quinone-COFs with MnO_2 and serve as cathode catalysts in Li-CO_2 batteries with a high discharge capacity (42,802 mAh/g at 200 mA/g) and good durability in rapid cycling tests.

Jiang et al., Cell Reports Physical Science 2, 100392
April 21, 2021 © 2021 The Author(s).
https://doi.org/10.1016/j.xcrp.2021.100392

Please cite this article in press as: Jiang et al., Exfoliation of covalent organic frameworks into MnO_2-loaded ultrathin nanosheets as efficient cathode catalysts for Li-CO_2 batteries, Cell Reports Physical Science (2021), https://doi.org/10.1016/j.xcrp.2021.100392

Cell Reports
Physical Science

CellPress
OPEN ACCESS

Article

Exfoliation of covalent organic frameworks into MnO_2-loaded ultrathin nanosheets as efficient cathode catalysts for Li-CO_2 batteries

Cheng Jiang,[1,4] Yu Zhang,[1,4] Mi Zhang,[1,4] Na-Na Ma,[3] Guang-Kuo Gao,[1] Jian-Hui Wang,[1] Meng-Meng Zhang,[1] Yifa Chen,[1,*] Shun-Li Li,[1,*] and Ya-Qian Lan[1,2,5,*]

SUMMARY

Rechargeable Li-CO_2 batteries have been studied extensively as an attractive strategy for simultaneous energy storage and CO_2 fixation to address the global environmental and energy crisis. However, state-of-the-art Li-CO_2 systems still suffer from unsatisfactory performance. Here, we successfully exfoliated quinone-based covalent organic frameworks (COFs) into large-scale and ultrathin MnO_2/2,6-diaminoanthraquinone-2,4,6-triformylphloroglucinol (DQTP)-COF-nanosheet (NS) hybrid materials. The obtained ultrathin nanosheets (as thin as 1.87 nm) synergistically integrate quinone-COF-NSs with MnO_2 and serve as powerful cathode catalysts in Li-CO_2 batteries. MnO_2/DQTP-COF-NS-3 has a high discharge capacity of 42,802 mAh/g at 200 mA/g. Additionally, it is durable for higher-stress test with a negligible change of overpotential from 500 to 1,000 mA/g and is discharged/charged rapidly for 120 cycles at 1 A/g. Moreover, the CO_2 activation mechanism is discussed and supported by density functional theory (DFT) calculations. This work may pave a new way for exploring porous crystalline materials as efficient cathode catalysts for Li-CO_2 batteries.

INTRODUCTION

Human activity has led to annual increases in global CO_2 concentration; the value of this in the atmosphere was 415 ppm in 2019, and it is approaching the warning line of 450 ppm.[1] It has triggered a series of problems like rising sea levels, an abnormal climate, ocean storms, increased desertification, etc.[2] Development of novel strategies like green conversion of CO_2 into renewable energy through environmentally friendly techniques is crucial for sustainable development of human society.[3] As one of the most promising and innovative energy storage strategies, Li-CO_2 batteries that can capture CO_2 and simultaneously store electrical energy have attracted tremendous attention because of their higher theoretical energy density (1,876 Wh kg^{-1}) compared with Li-ion batteries ($\approx$265 Wh kg^{-1}).[4] Specifically, Li-CO_2 batteries can be a desirable solution for power supplies in certain scenarios with high CO_2 concentration, such as factories, power plants, and even terraforming on Mars (96 vol % of CO_2 in the atmosphere).[5,6] However, several critical challenges, such as low energy efficiency, poor rate capacity, and short cycle life have largely limited practical applications of Li-CO_2 batteries. Development of novel materials and a deeper fundamental understanding of the structure-activity relationships are desired to advance the field.

In Li-CO_2 batteries, the CO_2 cathode is the core component for CO_2 capture and energy conversion, in which CO_2 is reduced and, typically, Li_2CO_3 is generated during

[1] Jiangsu Collaborative Innovation Centre of Biomedical Functional Materials, Jiangsu Key Laboratory of New Power Batteries, School of Chemistry and Materials Science, Nanjing Normal University, Nanjing 210023, P.R. China

[2] School of Chemistry, South China Normal University, Guangzhou 510006, P.R. China

[3] School of Chemistry and Chemical Engineering, Henan Normal University, Xinxiang, Henan 453007, P.R. China

[4] These authors contributed equally

[5] Lead contact

*Correspondence: chyf927821@163.com (Y.C.), slli@njnu.edu.cn (S.-L.L.), yqlan@njnu.edu.cn (Y.-Q.L.)

https://doi.org/10.1016/j.xcrp.2021.100392

the discharge reaction.[7] The major challenge when designing high-efficiency CO_2 electrodes stems from CO_2 capture/activation (CO_2 reduction reaction [CRR]) and decomposition of the discharge products like Li_2CO_3 (CO_2 evolution reaction [CER]).[8] Specifically, Li_2CO_3, a kind of wide band gap insulator is thermodynamically unfavorable, and constant deposition of it will cause the battery to expand and result in a CO_2 capture barrier, poor conductivity, or burying of catalysis sites, which generally require a high charge potential to decompose (usually more than 4.3 V versus Li/Li^+).[9] Therefore, it is desirable to develop powerful cathode catalysts to catalyze and improve the CRR/CER kinetics. We propose that powerful cathode catalysts for Li-CO_2 batteries would have the following advantages: (1) ability to capture, enrich, and activate CO_2; (2) fast electron and Li-ion transfer pathways; (3) efficient CRR/CER kinetics; (4) good cycling performance in a rapid discharge/charge process; and (5) a clear structure-to-property mechanism based on tunable composition or structure. To date, many cathode catalysts have been explored, such as porous carbon-based materials,[10–13] precious metals,[14–17] transition metal and oxides,[18–20] metal-organic frameworks (MOFs),[21] and covalent organic frameworks (COFs).[22,23] Among them, COFs are an emerging class of porous crystalline polymers constructed from molecular building blocks that are linked and extended periodically via strong covalent bonds and have been considered promising electrode candidates because of their high stability, open channels, and ease of functionalization.[24,25] COFs are promising and alternative materials in Li-CO_2 batteries mostly for the following reasons: the channels in COFs can be designed and controlled to serve as suitable diffusion pathways for Li ions and CO_2;[26–28] the structure of COFs can be functionalized with diverse functional groups or metal centers for efficient capture or activation of CO_2;[29] COFs can be hybridized with other materials to obtain functional composites with a synergistic effect to improve battery performance, and the clear crystal structure provides a desired platform to investigate the mechanism of Li-CO_2 batteries.

Currently, application of COFs in Li-CO_2 batteries is still in the early stage, generally applying COFs as porous substrates in the few existing examples, and the advantages of COFs have not yet been well exploited.[22,23] Additionally, the COFs reported in Li-CO_2 batteries are commonly in bulk form, with inefficient mass transfer and utilization of active sites. Therefore, we propose to assemble quinone-COF based nanosheets (quinone-COF-NSs) with typical metal oxide catalysts like MnO_2 to design well-dispersed hybrid materials. The corresponding considerations are as follows: (1) MnO_2, a common catalyst for Li-CO_2 batteries, is beneficial for CRR/CER;[30–33] (2) quinone groups, which can facilitate electron transfer and CO_2 activation, might be favorable for the interaction with CO_2;[34] (3) porous NS morphology, possessing the functions of nanoenrichment and nanoconfinement, can enhance electron and lithium ion conduction by shortening the tough diffusion path among CO_2 molecules and ensure uniform dispersion to avoid large Li_2CO_3 formation;[35,36] and (4) synergistic integration of quinone-COF-NSs with MnO_2 will presumably create a powerful catalysis system in which the 1D channel favors mass transfer and quinone groups facilitate electron transfer and CO_2 activation, allowing fast CRR/CER kinetics at the interface of quinone-COF-NSs and MnO_2 (Figure 1). From the above, we deduce that the hybrid materials of quinone-COF-NSs and MnO_2 may be promising candidates to enhance the performance of Li-CO_2 batteries, but exploration of these types of materials has been reported only rarely.

Here we report a series of large-scale and ultrathin MnO_2/2,6-diaminoanthraquinone-2,4,6-triformylphloroglucinol (DQTP)-COF-NS hybrid materials prepared successfully using a $KMnO_4$-based chemical exfoliation method (Figure 1). In this

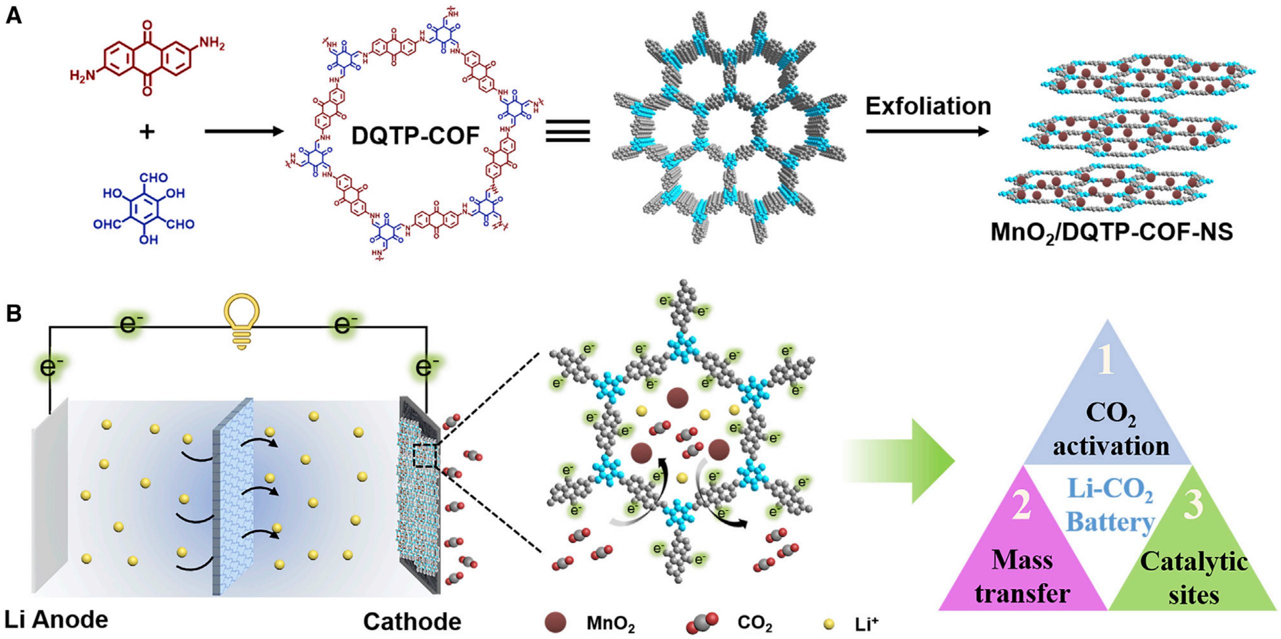

Figure 1. Schematic representation of the synthesis route for MnO_2/DQTP-COF-NSs and their advantages in Li-CO_2 batteries

(A) The chemical exfoliation of DQTP-COF into NSs.

(B) The advantages of MnO_2/DQTP-COF-NSs as cathode catalysts in Li-CO_2 batteries.

process of exfoliation, MnO_2 nanoparticles formed from $KMnO_4$ can be loaded uniformly loaded on NSs and inhibit agglomeration. By regulating the amount of $KMnO_4$, a series of ultrathin MnO_2/DQTP-COF-NSs with tunable MnO_2 loading and thickness are produced. The obtained materials possess ultrathin morphology (as thin as 1.87 nm over a large piece of NS; width, ~500 nm), well-developed porosity, numerous quinone groups, and uniformly dispersed MnO_2 and are promising alternatives as cathode catalysts for Li-CO_2 batteries. As expected, MnO_2/DQTP-COF-NS hybrid materials exhibit excellent performance as cathode catalysts in Li-CO_2 batteries. The best of them, the MnO_2/DQTP-COF-NS-3-based cell, delivers a large specific capacity of 42,802 mAh/g within 2.0–4.5 V at 200 mA/g, which is highest among porous coordination polymer-based catalysts. Additionally, the MnO_2/DQTP-COF-NS-3-based Li-CO_2 battery can be discharged and charged rapidly for 120 cycles with a cutoff capacity of 1,000 mAh/g at 1 A/g. Our findings provide valuable design principles for building powerful COF-based cathode catalysts with high performance.

RESULTS

Characterization of MnO_2/DQTP-COF-NS hybrid materials

MnO_2/DQTP-COF-NS hybrid materials were prepared using a $KMnO_4$-based chemical exfoliation method (for details, see Experimental procedures).[37] During the process, the as-synthesized DQTP-COF was exfoliated with various amounts of $KMnO_4$, giving MnO_2/DQTP-COF-NS-x (x = 1–4). The crystal phases of samples were first resolved using powder X-ray diffraction (PXRD) measurements. The as-synthesized DQTP-COF presents a series of characteristic signals at 3.5° and 7.0° and a broad peak at 26.7°, in accordance with the *P*6/m space group of DQTP-COF, which represents a hexagonal 2D layered network with an eclipsed AA stacking mode (Figure S1). After exfoliation, the peak at 3.5° disappeared, which might be attributed to exfoliation of DQTP-COF into lower dimensionality. Additionally, new peaks at

Please cite this article in press as: Jiang et al., Exfoliation of covalent organic frameworks into MnO_2-loaded ultrathin nanosheets as efficient cathode catalysts for Li-CO_2 batteries, Cell Reports Physical Science (2021), https://doi.org/10.1016/j.xcrp.2021.100392

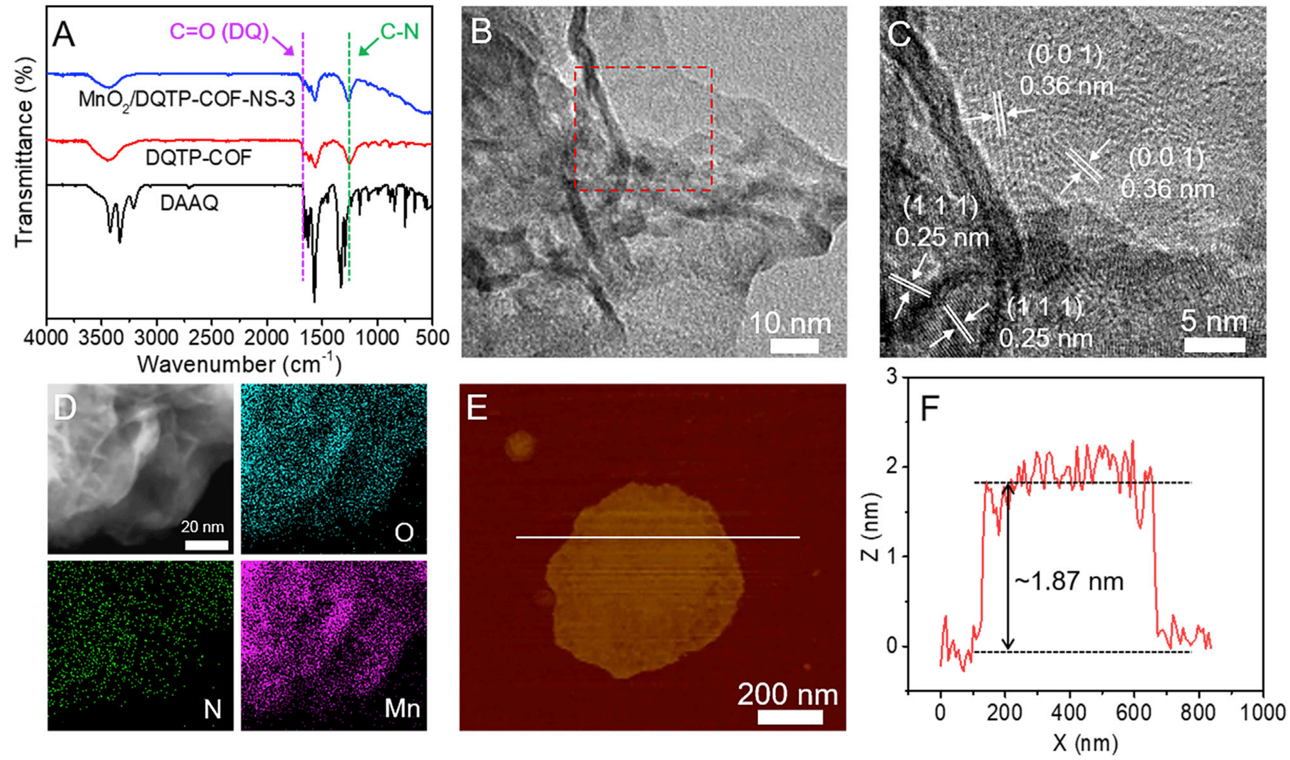

Figure 2. Characterization of MnO_2/DQTP-COF-NS-3

(A) FTIR spectra.

(B) TEM image.

(C) Enlarged image of the area outlined in (B).

(D) EDS elemental mapping images of O, N, and Mn.

(E) AFM topography image.

(F) Height profile of the line in (E).

36.7° and 65.8°, ascribed to birnessite-type δ-MnO_2 (JCPDS 80-1098) emerged after exfoliation, suggesting transformation of $KMnO_4$ into MnO_2 during the exfoliation process.[38] The peak intensity of MnO_2 increased gradually with the enhanced amount of $KMnO_4$ (Figure S1). To determine the percentage of MnO_2, thermogravimetric analyses (TGAs) were conducted, during which Mn was changed into Mn_2O_3 (JCPDS 65-7467) at 800°C, as supported by PXRD tests (Figure S2). Based on the TGA results, MnO_2 contents were calculated to be 1.0, 6.6, 18.9, and 36.3 wt % in MnO_2/DQTP-COF-NS-x (x = 1–4), respectively (Figure S3; Table S1). X-ray photoelectron spectroscopy (XPS) tests were carried out to determine the surface electronic state and elemental composition of Mn in MnO_2/DQTP-COF-NSs. Using MnO_2/DQTP-COF-NS-3 as an example, the result shows that the Mn element is tetravalent with two binding energies (i.e., 653.5 eV and 641.8 eV) ascribed to Mn $2p_{1/2}$ and Mn $2p_{3/2}$, respectively (Figure S4).

In addition, Fourier transform infrared (FTIR) spectra and ^{13}C solid-state nuclear magnetic resonance (ssNMR) measurements were performed to reveal the retained structure of DQTP-COF in MnO_2/DQTP-COF-NS hybrid materials. Using MnO_2/DQTP-COF-NS-3 as an example, the absorption peaks at 1,259 cm^{-1} and 1,671 cm^{-1} confirm successful formation of C-N and C = O (DAAQ) bonds, respectively, in the structure of DQTP-COF (Figure 2A). Upon exfoliation with various amounts of $KMnO_4$, the C-N and C = O bonds still exist, proving that the structure of DQTP-COF in MnO_2/DQTP-COF-NS-x (x = 1–4) was retained during the exfoliation process (Figure S5). Nevertheless, the C-N and C = O bonds disappear in MnO_2/DQTP-COF-NS-5 when an excessive amount of $KMnO_4$ added, suggesting that proper amounts of $KMnO_4$ can be applied successfully to exfoliate DQTP-COF while maintaining structural integrity (Figure S5). In the ^{13}C NMR spectrum of MnO_2/DQTP-COF-NS-3 (after acid treatment to remove MnO_2), the signals at 144 ppm correspond to the enamine carbon (= CNH), implying that the exfoliation process prefers to break the π-π interactions between the layers in DQTP-COF rather than destroy the 2D network reinforced by an irreversible β-ketoenamine-based covalent bond together with an H-bond (Figure S6).[26]

The morphology of the obtained samples was characterized by scanning electron microscopy (SEM) and transmission electron microscopy (TEM). DQTP-COF displays a bulk and aggregated morphology with a particle size of more than 1 μm, as supported by SEM and TEM (Figure S7). After exfoliation, bulk DQTP-COF was exfoliated into ultrathin NSs with largely decreased thickness, as shown by TEM (Figures 2B and S8–S10). Using MnO_2/DQTP-COF-NS-3 as an example, the bulk DQTP-COF was transferred into ultrathin NS morphology, as observed in the TEM image (Figure 2B). To detect the thickness of the samples, atomic force microscope (AFM) tests were conducted. Specifically, the thickness of MnO_2/DQTP-COF-NS-3 was ~1.87 nm over a large piece of NS (width, ~500 nm), much thinner than that of DQTP-COF, which can be ascribed to a layer thickness of ~6 molecules (Figures 2E and 2F). The thicknesses of the MnO_2/DQTP-COF-NS-x (x = 1, 2, and 4) was 4.58 nm, 3.54 nm, and 5.76 nm, respectively (Figure S11). High-resolution (HR) TEM imaging reveals that the lattice fringe distances of 0.25 and 0.36 nm can be assigned to the (111) plane of MnO_2[38] and (001) plane of DQTP-COF, respectively, indicating integration of MnO_2 and DQTP-COF in MnO_2/DQTP-COF-NS-3 (Figure 2C). Energy-dispersive X-ray spectroscopy (EDS) mapping analysis reveals that Mn, N, and O are distributed uniformly in the NSs (Figure 2D).

The porosity of the samples obtained with ultrathin NS morphology was confirmed by gas sorption tests. The Brunauer-Emmett-Teller surface area (S_{BET}) of MnO_2/DQTP-COF-NS-x (x = 1–4) was calculated to be 223, 84, 75, and 138 $m^2\ g^{-1}$, respectively—lower than that of bulk DQTP-COF (S_{BET}, 411 $m^2\ g^{-1}$) (Figure S12). After exfoliation, the decrease in S_{BET} was possibly due to transformation of COFs into lower dimensionality, and the change in S_{BET} might be closely related to the NS thickness that more defects will be generated in samples with lower ones, thus leading to the decrease in S_{BET}. The pore volume (V_t) of MnO_2/DQTP-COF-NS-x (x = 1–4) was 0.25, 0.14, 0.17, and 0.29 $cm^3\ g^{-1}$, respectively (Table S2). Furthermore, the CO_2 adsorption capacity of MnO_2/DQTP-COF-NS-x (x = 1–4) was 29, 20, 16, and 12 $cm^3\ g^{-1}$ at 298 K, slightly lower than that of DQTP-COF (44 $cm^3\ g^{-1}$) (Figure S13).

Electrochemical performance of Li-CO_2 batteries

As mentioned above, we successfully synthesized a series of MnO_2/DQTP-COF-NS-x (x = 1–4) hybrid materials with tunable NS morphology and MnO_2 loadings. To determine the effect of different loadings of MnO_2 on the Li-CO_2 system, the initial battery properties of these samples as cathode catalysts were evaluated. Figure S14 shows the discharge/charge curves of relative electrodes cycled at a constant current density of 200 mA/g with a fixed capacity of 1,000 mAh/g. MnO_2/DQTP-COF-NS-x (x = 1–3) have a slight change discharge platform, higher than that of MnO_2/DQTP-COF-NS-4 with excessive loading of MnO_2 (Figure S15). MnO_2/DQTP-COF-NS-1 with the lowest MnO_2 loading (1.0 wt %) has the highest charge platform (4.40 V). MnO_2/DQTP-COF-NS-2 (4.29 V) and MnO_2/DQTP-COF-NS-4 (4.38 V) have slightly lower charge platforms than MnO_2/DQTP-COF-NS-3 (4.18 V). Notably, the MnO_2/DQTP-COF-NS-3

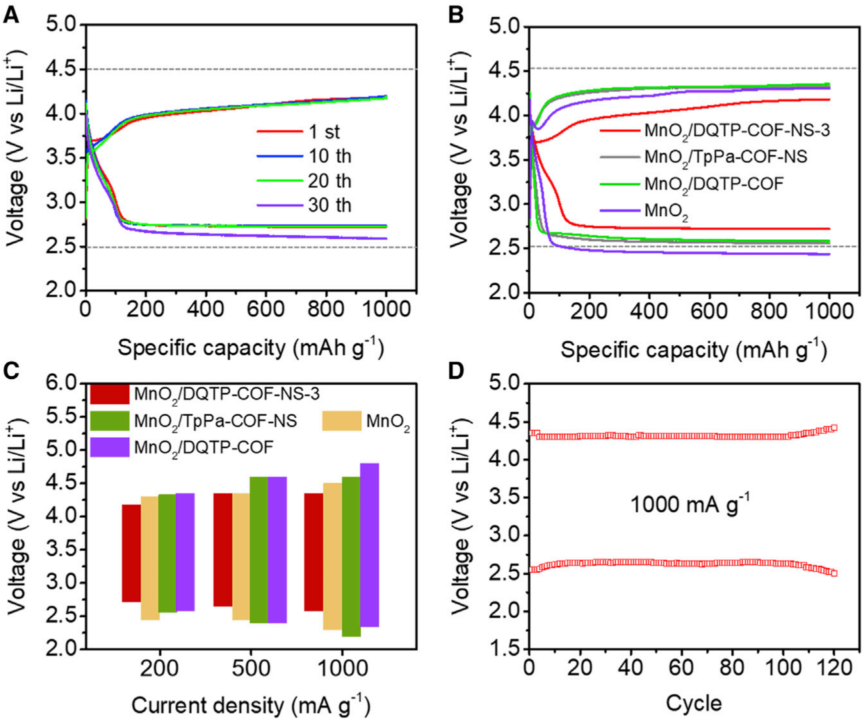

Figure 3. Electrochemical performance of Li-CO_2 batteries

(A) Discharge/charge cycling curves of MnO_2/DQTP-COF-NS-3 with a limited capacity of 1,000 mAh/g at 200 mA/g.

(B) Discharge/charge curves of the first cycle with a limited capacity of 1,000 mAh/g at 200 mA/g with different cathode catalyst materials.

(C) The discharge/charge potentials of different cathodes at current densities of 200 mA/g, 500 mA/g, and 1,000 mA/g with different cathode catalyst materials.

(D) Long-term cycling curve of the MnO_2/DQTP-COF-NS-3 cathode catalyst at 1,000 mA/g.

cathode shows much better catalytic activity with the highest discharged potential (2.72 V) and lowest charged potential (4.18 V), possibly because of the moderate MnO_2 loading and thinnest NS morphology (Figure S15).

To reveal the effect of quinone groups and well-tuned NS morphology on performance, various contrast samples, like TpPa-COF, DQTP-COF and a physical mixture of DQTP-COF and MnO_2, were prepared. TpPa-COF, consisting of para-phenylenediamine (Pa) and 2,4,6-triformylphloroglucinol (TFP), displayed similar structure as DQTP-COF, except that without quinone groups, and was synthesized and exfoliated into NSs (called MnO_2/TpPa-COF-NS), as verified by PXRD pattern, FTIR spectra, and SEM and TEM images (Figures S16–S20).[39] To confirm the superiority of MnO_2/DQTP-COF-NS-3, three kinds of cathode catalysts (DQTP-COF, MnO_2/DQTP-COF-NS-3, and MnO_2/TpPa-COF-NS) were tested, following similar electrochemical methods at 200 mA/g with a fixed capacity of 1,000 mAh/g (Figure 3B). DQTP-COF and MnO_2/DQTP-COF-NS-3 have similar and relatively high discharge terminal potentials of 2.72 V at the first cycle, which probably results from the presence of quinone moieties. In comparison, MnO_2/TpPa-COF-NS has a lower discharge potential of 2.56 V and discharged down to 2.32 V at the 30th cycle, indicating intensified polarization of the battery (Figure S21). MnO_2/DQTP-COF-NS-3 and DQTP-COF cathodes showed slight changes in potential plateau, whereas MnO_2/TpPa-COF-NS had enlarged significantly in voltage hysteresis at the 30th cycle (Figures 3A and S21). It implies that quinone moieties are essential for improvement of Li-CO_2 performance, especially the discharge potential. Moreover, the DQTP-COF-based battery can be used within 2.7–4.5 V for cycling tests, illustrating that the high structure stability and efficient quinone moieties might contribute to performance (Figure S21). However, there is still a high charge potential with the DQTP-COF cathode (4.43 V), possibly because of the lack of MnO_2 and well-tuned NS morphology. As contrast sample, MnO_2 has a charge potential of 4.30 V with a low discharge potential of 2.45 V (Figures S22 and S23). Therefore, MnO_2/DQTP-COF-NS-3, as the integration sample of DQTP-COF and MnO_2 with NS morphology, shows higher performance than the single component. To further verify the importance of hybrid materials with ultrathin NS morphology, MnO_2/DQTP-COF (a physical mixture of DQTP-COF and MnO_2) was prepared as a contrast sample for MnO_2/DQTP-COF-NS-3 (Figure S24). As expected, when cycled galvanostatically at 200 mA/g, the MnO_2/DQTP-COF cathode discharged at 2.58 V and charged at 4.35 V of the first cycle (Figure S25).

The advantages of MnO_2/DQTP-COF-NS-3, in which numerous quinone groups and MnO_2 are distributed uniformly in the ultrathin NS, play a vital role in capacity performance. The specific capacity properties of MnO_2/DQTP-COF-NS-3, MnO_2/DQTP-COF, MnO_2/TpPa-COF-NS, and MnO_2 were evaluated using full discharge curves at a current density of 200 mA/g (Figure S26). The specific capacities of batteries with MnO_2/DQTP-COF-NS-3, MnO_2/DQTP-COF, MnO_2/TpPa-COF-NS, and MnO_2 were calculated to be 42,802, 20,410, 10,525 and 8,262 mAh/g, respectively. MnO_2/DQTP-COF-NS-3 exhibits a much higher specific capacity than the others, suggesting that the synergistic advantages of hybrid materials like ultrathin NS morphology, quinone groups, and uniformly distributed MnO_2 might be responsible for the excellent specific capacity. The specific capacity property of Ketjen Black (KB) was evaluated using a full discharge curve at 200 mA/g and was calculated to be 9380 mAh/g (Figures S27 and S28). The experimental result proves that KB has much less capacity contribution and that it mainly plays a role in electrical conductivity. As far as we know, MnO_2/DQTP-COF-NS-3 possesses the highest specific capacity among all of the reported porous coordination polymer-based Li-CO_2 batteries and is also superior to most cathode materials (Table S3).[8,9,21–23]

Li-CO_2 battery performance was also evaluated at large current densities. Figure 3C shows the discharge/charge potentials with different catalysts at current densities of 200, 500, and 1,000 mA/g with a fixed capacity of 1,000 mAh/g. The MnO_2/DQTP-COF-NS-3 cathode shows voltage hysteresis of 1.46 V, 1.75 V, and 1.77 V at 200, 500, and 1,000 mA/g, respectively. The negligible change in voltage hysteresis at current densities from 500–1,000 mA/g indicates that the cathode catalyst can be durable in a higher-stress test in the Li-CO_2 system. The MnO_2/DQTP-COF-NS-3 cathode has a higher discharge potential and lower charge potential compared with other catalysts at all current densities, which is mainly due to the excellent CRR/CER catalytic activity (Figure 3C). The battery cycling tests of MnO_2/DQTP-COF-NS-3, examined at high current densities of 500 and 1,000 mA/g with a limited capacity of 1,000 mAh/g, display long-term stable performance during 100 cycles at 500 mA/g and 120 cycles at 1,000 mA/g, respectively (Figures 3D and S29). These results show that combination of DQTP-COF NS with MnO_2 can efficiently narrow down the overpotential and enhance the battery kinetics, allowing the battery to run longer cycles and endure higher current densities.

In addition, the conductive agent KB as a conductive additive was also tested. Figure S28 shows the discharge/charge curves of KB at current densities of 200, 500, and 1,000 mA/g with a fixed capacity of 1,000 mAh/g. The KB cathode shows voltage hysteresis of 2.27 V, 2.47 V, and 2.71 V at 200, 500, and 1,000 mA/g, respectively

Please cite this article in press as: Jiang et al., Exfoliation of covalent organic frameworks into MnO_2-loaded ultrathin nanosheets as efficient cathode catalysts for Li-CO_2 batteries, Cell Reports Physical Science (2021), https://doi.org/10.1016/j.xcrp.2021.100392

(Figure S28). Experimental results show that KB has a much poorer battery performance during the cycling process compared with MnO_2/DQTP-COF-NS-3. Therefore, KB only acts as a conductive additive and has a minor effect on battery performance. To determine the effect of KB on the Li-CO_2 system, different ratios of KB in the cathode (MnO_2/DQTP-COF-NS-3: KB: PVDF, 5:4:1; 6:3:1; 7:2:1 and 8:1:1) were evaluated (Figure S30). The discharge/charge curves of relative electrodes were cycled at a constant current density of 200 mA/g with a fixed capacity of 1,000 mAh/g. Notably, the cathode with the best ratio of KB (MnO_2/DQTP-COF-NS-3: KB: PVDF = 7:2:1) had the highest discharged potential (2.72 V) and lowest charged potential (4.18 V). In addition, we performed the cell test based on carbonized paper, and no property was detected. The type of carbonized paper was Hesen HCP010N, and it was applied as the test sample without addition of catalyst. The first discharge/charge curve of bare carbonized paper cycled at 20 μA with a fixed capacity of 0.10 mAh was evaluated (Figure S31). The result shows a voltage hysteresis of 2.38 V. Therefore, carbonized paper only acts as the conductive substrate and has a negligible effect on battery performance. Moreover, the activity of MnO_2/DQTP-COF-NS-3 in CO_2 and Ar atmospheres was tested to verify the origin of Li-CO_2. Ar gas was applied to replace CO_2, and we tested the full discharge/charge of MnO_2/DQTP-COF-NS-3 at 200 mA/g. The results show that the discharge platform descends to 2.0 V with a low capacity of 900 mAh/g, and the charge platform quickly reaches 4.5 V (Figure S32).

A well-designed Li-CO_2 cathode catalyst must perform functions like capturing and enriching CO_2, restricting deposition of Li_2CO_3, and catalyzing decomposition of Li_2CO_3.[5] The poor stability of the Li-CO_2 battery is mainly caused by incomplete decomposition of Li_2CO_3 during the charging process, leading to diffusion channel clogging, cathode surface passivation, and battery performance degradation. In general, the morphology or particle sizes of the generated Li_2CO_3 on the cathode surface largely affects the charge process.[4] To investigate this, the discharge products at different stages of a discharge/charge cycle with a fixed capacity of 1,000 mAh/g and a voltage range of 2.0–4.5 V versus Li/Li^+ were characterized (Figure 4G). Three stages (pristine state, discharge to 1,000 mAh/g, and recharge during the discharge/charge cycle) were selected as desired examples. SEM was conducted to trace the formation and decomposition processes of Li_2CO_3 in the cathode. The pristine MnO_2/DQTP-COF-NS-3 and MnO_2/DQTP-COF cathodes display NS and bulk morphology with a small amount of particle-like KB on the carbon paper (Figures. 4A and 4D). Notably, after discharge, Li_2CO_3 with particle size of $\sim$100 nm was generated on the surface of the MnO_2/DQTP-COF-NS-3 cathode, which was much smaller than that on the MnO_2/DQTP-COF cathode (>250 nm) (Figures 4B and 4E). Further supported by the PXRD tests, new peaks at 21.2°, 30.5°, and 31.6° were ascribed to the (110), ($-$202), and (202) planes of Li_2CO_3 crystals (PDF 22-1411) in the state of discharge to 1,000 mAh/g, suggesting that crystalline Li_2CO_3 was the main discharge product of the batteries (Figure 4H). The Li_2CO_3 generated on the MnO_2/DQTP-COF-NS-3 cathode was much looser than that on the MnO_2/DQTP-COF cathode, indicating that the advantages of MnO_2/DQTP-COF-NS-3 with ultrathin NS morphology and quinone groups might have a synergistic effect on the CRR process (Figures 4B and 4E). After that, Li_2CO_3 is completely decomposed on the MnO_2/DQTP-COF-NS-3 cathode in the state of recharge (Figure 4C). In contrast, the Li_2CO_3 is incompletely decomposed on the MnO_2/DQTP-COF cathode after the recharge process, as shown by SEM and PXRD (Figures 4F and S33).

Electrochemical impedance spectroscopy (EIS) was conducted to evaluate battery impedance. Figure S34 displays the EIS spectra of the MnO_2/DQTP-COF-NS-3 catalyst-based Li-CO_2 battery before discharge, after the first discharge, and after the first recharge. The results show a dramatic increase in battery impedance when

Please cite this article in press as: Jiang et al., Exfoliation of covalent organic frameworks into MnO_2-loaded ultrathin nanosheets as efficient cathode catalysts for Li-CO_2 batteries, Cell Reports Physical Science (2021), https://doi.org/10.1016/j.xcrp.2021.100392

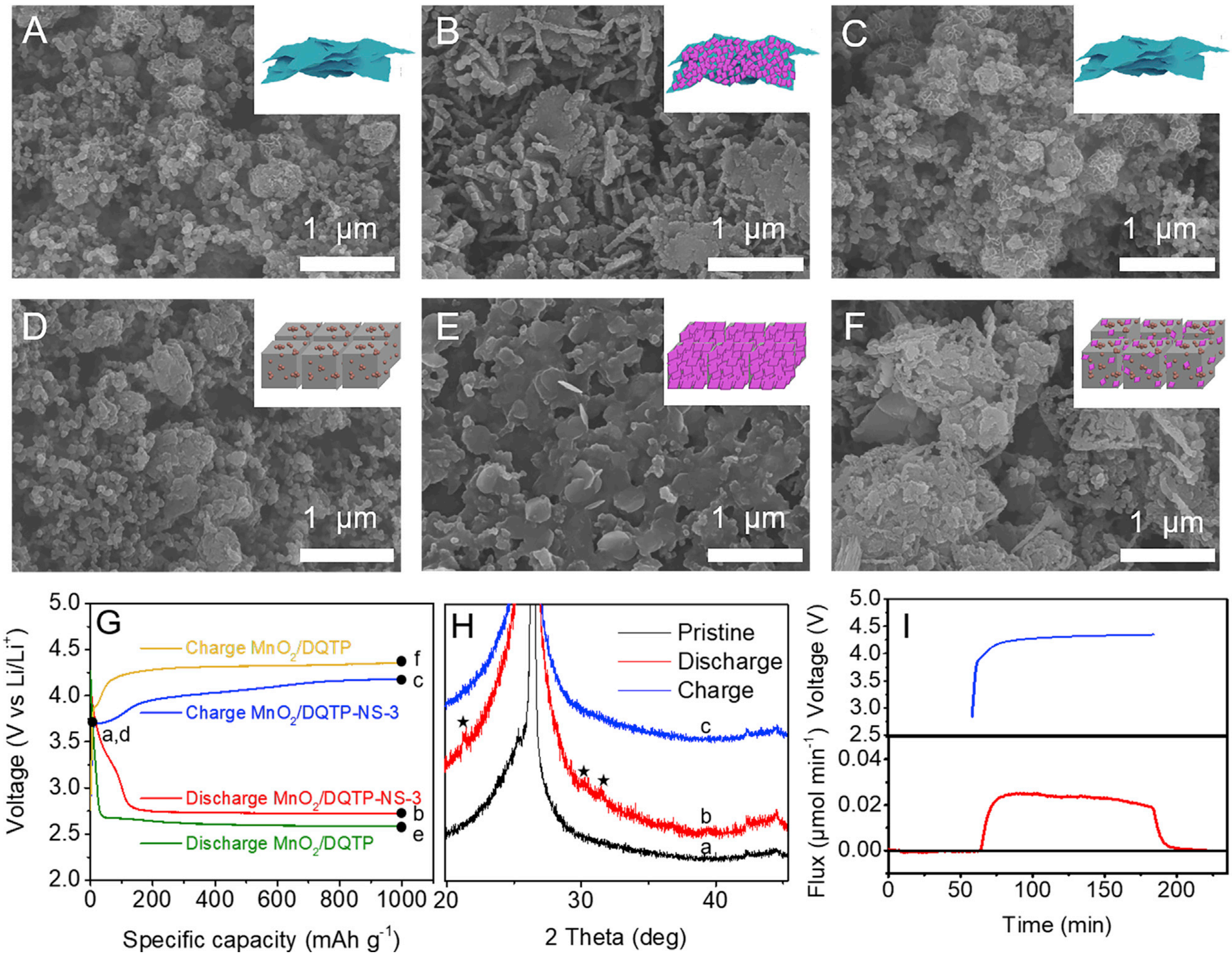

Figure 4. Li_2CO_3 tracing tests in the first discharge/recharge process with a limited capacity of 1,000 mAh/g at 200 mA/g

(A–C) SEM images of MnO_2/DQTP-COF-NS-3 in three stages (pristine, discharge, and charge).

(D–F) SEM images of MnO_2/DQTP-COF in three stages (pristine, discharge, and charge).

(G) First discharge/charge curves with the MnO2/DQTP-COF-NS-3 or MnO2/DQTP-COF cathode

(H) PXRD patterns of MnO_2/DQTP-COF-NS-3.

(I) DEMS of MnO_2/DQTP-COF-NS-3 upon discharge and recharge at 1,000 mA/g.

compared the initial state with the first discharge one because of deposition of insulating Li_2CO_3 on the surface of the cathode (Figure S34). Excessive coverage of Li_2CO_3 on the cathode surface could lead to sudden death of the Li-CO_2 battery. MnO_2/DQTP-COF-NS-3, serving as a high electrocatalytic activity cathode catalyst with ultrathin NS morphology coupled with multifunctionality, is beneficial for uniform deposition and complete decomposition of insulating Li_2CO_3, facilitating full recovery of impedance in the battery. Subsequently, *in situ* differential electrochemical mass spectrometry (DEMS) was adopted to monitor the gas evolution of the cell with the MnO_2/DQTP-COF-NS-3 cathode during the charge process (Figure 4I).[31] The DEMS spectra show that the cell releases CO_2 upon the charge process without any trace of O_2. The charge-to-mass ratio during charging was determined to be $4.1e^-/3CO_2$, which is close to the theoretical value of $4e^-/3CO_2$, indicating that the process well matches the reversible reaction $4Li^+ + 3CO_2 + 4e^- \rightarrow 2Li_2CO_3 + C$.[40] EIS and DEMS confirm that fully reversible MnO_2/DQTP-COF-NS-3-based Li-CO_2 batteries hold much promise as high-performance cathode catalysts.

Please cite this article in press as: Jiang et al., Exfoliation of covalent organic frameworks into MnO_2-loaded ultrathin nanosheets as efficient cathode catalysts for Li-CO_2 batteries, Cell Reports Physical Science (2021), https://doi.org/10.1016/j.xcrp.2021.100392

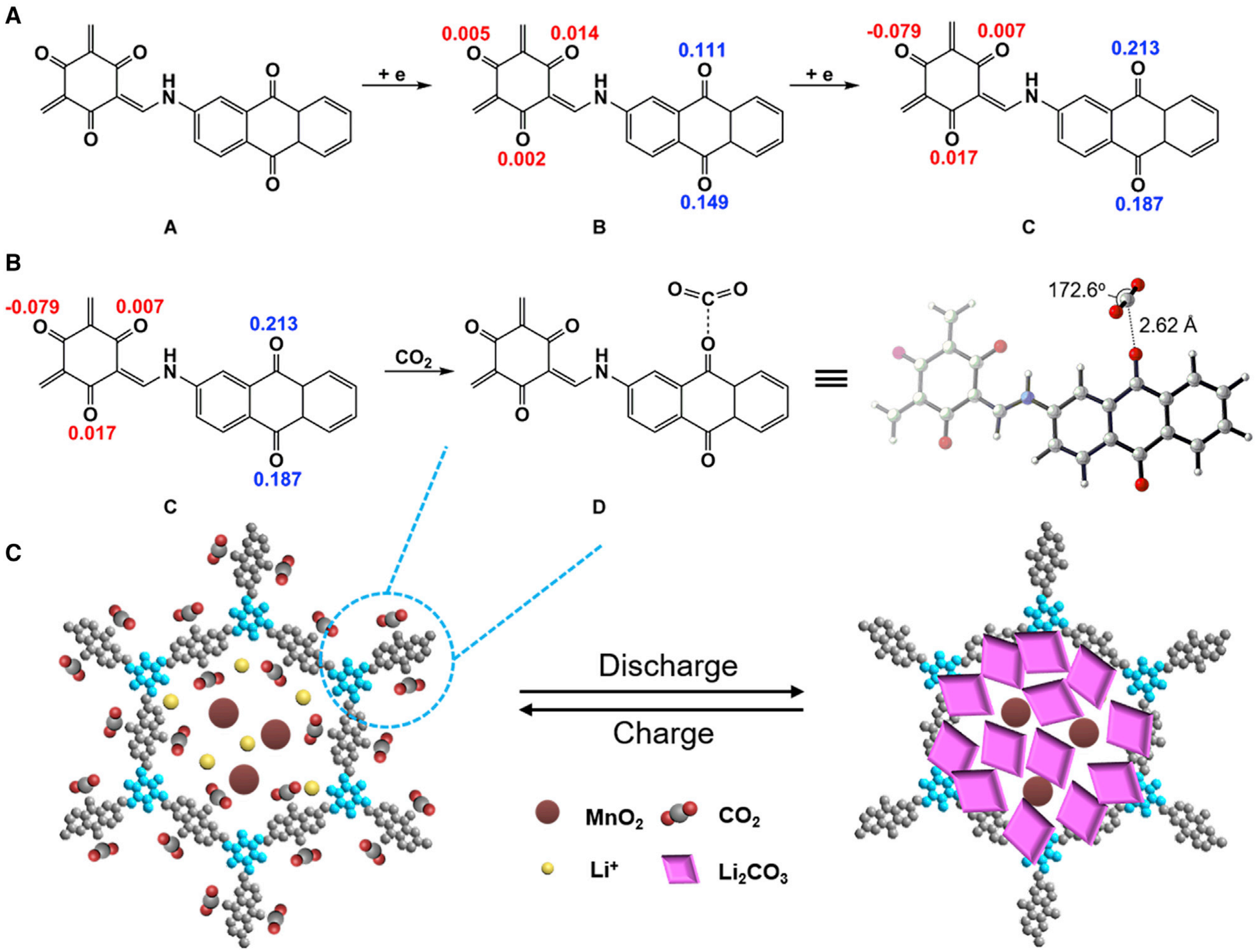

Figure 5. DFT calculations of the interaction between CO_2 and the quinone moiety in MnO_2/DQTP-COF-NS

(A) Calculated model (A) and spin density distribution of reduced forms (B and C) during the electron-gaining process.

(B) Schematic representation of the CO_2 activation process (the optimized structure [D] and selected parameters).

(C) Schematic representation of MnO_2/DQTP-COF-NS during the discharge and charge process (the circle area indicates model D).

All calculations were performed using the Gaussian 09 program, and functional B3LYP was used with a standard 6–31+G(d) basis set to optimize the geometries of all structures.

Density functional theory calculations

Based on the results mentioned above, quinone groups, having a positive effect on CO_2 activation and interaction, facilitate the CRR process to improve Li-CO_2 battery performance. To verify this, density functional theory (DFT) calculations were performed to investigate the vital role of quinone moieties in reduction of CO_2. All calculations were performed using the Gaussian 09 program,[41] and functional B3LYP was used with a standard 6–31+G(d) basis set to optimize the geometries of all structures. We selected a repeat unit A of DQTP-COF as a computation model to investigate the interaction with CO_2 (Figure 5A). In general, CO_2 activates one electron, and the activation process has a high free energy (ΔG) of 18.5 kcal/mol, resulting in slow CRR kinetics in Li-CO_2 batteries.[34] The calculated spin density values of forms B and C indicate that the first and second electrons are focused on the oxygen of quinone rather than the oxygen in TFP (Figure 5A). Subsequently, the interaction of CO_2 and the quinone moiety was calculated. The selected parameters of optimized structure D are shown in Figure 5B and imply interaction between CO_2 and the reduced form C. During the process, the CO_2 molecule is slightly twisted, and the angle

Please cite this article in press as: Jiang et al., Exfoliation of covalent organic frameworks into MnO_2-loaded ultrathin nanosheets as efficient cathode catalysts for Li-CO_2 batteries, Cell Reports Physical Science (2021), https://doi.org/10.1016/j.xcrp.2021.100392

changed to 172.6° with a distance of 2.62 Å, calculated from CO_2 to the oxygen of the quinone moiety. The interaction process for CO_2 has a ΔG of 9.5 kcal/mol, which is much lower than that of $CO_2 \rightarrow CO_2^{\bullet -}$. The selected nature population analysis (NPA) charges of C and D also illustrate that electron transfer occurs between quinone and CO_2 (Figure S36). The CO_2 absorption before the electron injection was also considered, and the ΔG value was 5.0 kcal/mol (Figure S35), but the NPA charges hardly changed after interaction with CO_2 (see charges of A and E in Figure S36). Combined with the angle of 178.3° of CO_2 and a distance of 3.00 Å from CO_2 to the oxygen of the quinone moiety in E, this suggests that A hardly activates CO_2 before the electron injection. Moreover, the electron reduction process $A \rightarrow C$ has a ΔG value of -51.1 kcal/mol, which is a more reasonable process than that of A directly combined with CO_2 to become E ($\Delta G = 5$ kcal/mol) (Figure S35). Therefore, quinone groups indeed serve have a vital role in activation of CO_2, which is important for improvement of Li-CO_2 battery performance. Based on the DFT results, we can propose a possible basic mechanism of these cathode catalysts in Li-CO_2 batteries (Figure 5). First, quinone groups in DQTP-COF get the electrons and convert them into an intermediate reduction state. Subsequently, the quinone groups in the reduction state interact with CO_2 to form kinds of stable quinone-CO_2 adducts that possess a much lower free energy compared with the direct process of $CO_2 \rightarrow CO_2^{\bullet -}$. In the presence of Li ions, CO_2 could be reduced further to solid products (e.g., Li_2CO_3 and C) during the discharge process. Specifically, Li_2CO_3 in small sizes is distributed evenly on the surface of ultrathin NSs based on the above results. Finally, the generated Li_2CO_3 can be decomposed efficiently at the interface of quinone-COF-NSs and MnO_2 during the charging process (Figure 5C).

DISCUSSION

We successfully exfoliated quinone-based COFs into large-scale and ultrathin MnO_2/DQTP-COF-NS hybrid materials using a $KMnO_4$-based chemical exfoliation method. The obtained materials possess ultrathin morphology (as thin as 1.87 nm over a large piece of NS; width, ~500 nm), well-developed porosity, numerous quinone groups, and uniformly dispersed MnO_2 and are promising alternatives for cathode catalysts for Li-CO_2 batteries. Specifically, the synergistic effect of COF NSs with quinone moieties and MnO_2 can efficiently narrow down the overpotential and enhance CRR/CER kinetics, allowing the battery to run longer cycles and endure higher current densities. The MnO_2/DQTP-COF-NS-3-based cell delivers a large specific capacity of 42,802 mAh/g within 2.0–4.5 V at 200 mA/g, which is highest among porous coordination polymer-based catalysts. The MnO_2/DQTP-COF-NS-3-based Li-CO_2 battery can be durable in a higher-stress test with negligible change of overpotential at current densities from 500–1,000 mA/g and can be discharged and charged rapidly for 120 cycles at 1 A/g. Moreover, the CO_2 activation mechanism was discussed, as supported by DFT calculations. This work paves a new way for exploring porous crystalline materials as efficient cathode catalysts for Li-CO_2 batteries, which might extend the scope of applicable materials in this area.

EXPERIMENTAL PROCEDURES

Resource availability

Lead contact

Further information and requests for resources and reagents should be directed to and will be fulfilled by the lead contact, Ya-Qian Lan (yqlan@njnu.edu.cn).

Materials availability

This study did not generate new unique reagents.

Data and code availability

The authors declare that the data supporting the findings of this study are available in the article and the supplemental information. All other data and codes are available from the lead contact upon reasonable request.

General procedures

Full descriptions of all synthesis, characterization, and electrochemical measurements can be found in the supplemental experimental procedures.

SUPPLEMENTAL INFORMATION

Supplemental information can be found online at https://doi.org/10.1016/j.xcrp.2021.100392.

ACKNOWLEDGMENTS

This work was financially supported by NSFC (21871141, 21871142, 21701085, and 21901122); the NSF of Jiangsu Province of China (BK20171032); the Natural Science Research of Jiangsu Higher Education Institutions of China (17KJB150025 and 19KJB150011); and a project funded by the China Postdoctoral Science Foundation (2018M630572 and 2019M651873), Priority Academic Program Development of Jiangsu Higher Education Institutions, and the Foundation of Jiangsu Collaborative Innovation Center of Biomedical Functional Materials.

AUTHOR CONTRIBUTIONS

Y.-Q.L., Y.C., and C.J. conceived and designed the idea. C.J., M.Z., and Y.Z. designed the experiments and collected and analyzed the data. N.-N.M. carried out the theoretical/DFT calculations. G.-K.G., J.-H.W., S.-L.L., and M.-M.Z. assisted with the experiments and characterizations. C.J. wrote the manuscript. C.J., Y.C., and Y.-Q.L. discussed the results and prepared the manuscript. All authors reviewed and contributed to this paper.

DECLARATION OF INTERESTS

The authors declare no competing interests.

Received: November 16, 2020
Revised: March 9, 2021
Accepted: March 15, 2021
Published: April 2, 2021

REFERENCES

1. Nehrbass-Ahles, C., Shin, J., Schmitt, J., Bereiter, B., Joos, F., Schilt, A., Schmidely, L., Silva, L., Teste, G., Grilli, R., et al. (2020). Abrupt CO_2 release to the atmosphere under glacial and early interglacial climate conditions. Science *369*, 1000–1005.
2. Yu, J., Xie, L.H., Li, J.R., Ma, Y., Seminario, J.M., and Balbuena, P.B. (2017). CO_2 Capture and Separations Using MOFs: Computational and Experimental Studies. Chem. Rev. *117*, 9674–9754.
3. Xie, J., and Wang, Y. (2019). Recent Development of CO_2 Electrochemistry from Li-CO_2 Batteries to Zn-CO_2 Batteries. Acc. Chem. Res. *52*, 1721–1729.
4. Mu, X., Pan, H., He, P., and Zhou, H. (2020). Li-CO_2 and Na-CO_2 Batteries: Toward Greener and Sustainable Electrical Energy Storage. Adv. Mater. *32*, e1903790.
5. Xie, Z., Zhang, X., Zhang, Z., and Zhou, Z. (2017). Metal-CO_2 Batteries on the Road: CO_2 from Contamination Gas to Energy Source. Adv. Mater. *29*, 1605891.
6. Li, J., Wang, L., Zhao, Y., Li, S., Fu, X., Wang, B., and Peng, H. (2020). Li-CO_2 Batteries Efficiently Working at Ultra-Low Temperatures. Adv. Funct. Mater. *30*, 2001619.
7. Chen, J., Zou, K., Ding, P., Deng, J., Zha, C., Hu, Y., Zhao, X., Wu, J., Fan, J., and Li, Y. (2019). Conjugated Cobalt Polyphthalocyanine as the Elastic and Reprocessable Catalyst for Flexible Li-CO_2 Batteries. Adv. Mater. *31*, e1805484.
8. Liu, B., Sun, Y., Liu, L., Chen, J., Yang, B., Xu, S., and Yan, X. (2019). Recent Advances in Understanding Li-CO_2 Electrochemistry. Energy Environ. Sci. *12*, 887–922.
9. Xie, J., Zhou, Z., and Wang, Y. (2020). Metal-CO_2 Batteries at the Crossroad to Practical Energy Storage and CO_2 Recycle. Adv. Funct. Mater. *30*, 1908285.
10. Zhang, Z., Zhang, Q., Chen, Y., Bao, J., Zhou, X., Xie, Z., Wei, J., and Zhou, Z. (2015). The First Introduction of Graphene to Rechargeable Li-CO_2 Batteries. Angew. Chem. Int. Ed. Engl. *54*, 6550–6553.

Please cite this article in press as: Jiang et al., Exfoliation of covalent organic frameworks into MnO_2-loaded ultrathin nanosheets as efficient cathode catalysts for Li-CO_2 batteries, Cell Reports Physical Science (2021), https://doi.org/10.1016/j.xcrp.2021.100392

11. Qie, L., Lin, Y., Connell, J.W., Xu, J., and Dai, L. (2017). Highly Rechargeable Lithium-CO_2 Batteries with a Boron- and Nitrogen-Codoped Holey-Graphene Cathode. Angew. Chem. Int. Ed. Engl. *56*, 6970–6974.
12. Jin, Y., Hu, C., Dai, Q., Xiao, Y., Lin, Y., Connell, J.W., Chen, F., and Dai, L. (2018). High-Performance Li-CO_2 Batteries Based on Metal-Free Carbon Quantum Dot/Holey Graphene Composite Catalysts. Adv. Funct. Mater. *28*, 1804630.
13. Li, X., Zhou, J., Zhang, J., Li, M., Bi, X., Liu, T., He, T., Cheng, J., Zhang, F., Li, Y., et al. (2019). Bamboo-Like Nitrogen-Doped Carbon Nanotube Forests as Durable Metal-Free Catalysts for Self-Powered Flexible Li-CO_2 Batteries. Adv. Mater. *31*, e1903852.
14. Yang, S., Qiao, Y., He, P., Liu, Y., Cheng, Z., Zhu, J.-J., and Zhou, H. (2017). A Reversible Lithium-CO_2 Battery with Ru Nanoparticles as a Cathode Catalyst. Energy Environ. Sci. *10*, 972–978.
15. Xing, Y., Yang, Y., Li, D., Luo, M., Chen, N., Ye, Y., Qian, J., Li, L., Yang, D., Wu, F., et al. (2018). Crumpled Ir Nanosheets Fully Covered on Porous Carbon Nanofibers for Long-Life Rechargeable Lithium-CO_2 Batteries. Adv. Mater. *30*, e1803124.
16. Qiao, Y., Xu, S., Liu, Y., Dai, J., Xie, H., Yao, Y., Mu, X., Chen, C., Kline, D.J., Hitz, E.M., et al. (2019). Transient, In-situ Synthesis of Ultrafine Ruthenium Nanoparticles for a High-rate Li-CO_2 Battery. Energy Environ. Sci. *12*, 1100–1107.
17. Xing, Y., Wang, K., Li, N., Su, D., Wong, W.-T., Huang, B., and Guo, S. (2020). Ultrathin RuRh Alloy Nanosheets Enable High-Performance Lithium-CO_2 Battery. Matter *2*, 1494–1508.
18. Zhang, Z., Wang, X.-G., Zhang, X., Xie, Z., Chen, Y.-N., Ma, L., Peng, Z., and Zhou, Z. (2017). Verifying the Rechargeability of Li-CO_2 Batteries on Working Cathodes of Ni Nanoparticles Highly Dispersed on N-Doped Graphene. Adv. Sci. (Weinh.) *5*, 1700567.
19. Qiao, Y., Liu, Y., Chen, C., Xie, H., Yao, Y., He, S., Ping, W., Liu, B., and Hu, L. (2018). 3D-Printed Graphene Oxide Framework with Thermal Shock Synthesized Nanoparticles for Li-CO_2 Batteries. Adv. Funct. Mater. *28*, 1805899.
20. Hu, C., Gong, L., Xiao, Y., Yuan, Y., Bedford, N.M., Xia, Z., Ma, L., Wu, T., Lin, Y., Connell, J.W., et al. (2020). High-Performance, Long-Life, Rechargeable Li-CO_2 Batteries based on a 3D Holey Graphene Cathode Implanted with Single Iron Atoms. Adv. Mater. *32*, e1907436.
21. Li, S., Dong, Y., Zhou, J., Liu, Y., Wang, J., Gao, X., Han, Y., Qi, P., and Wang, B. (2018). Carbon Dioxide in the Cage: Manganese Metal-Organic Frameworks for High Performance CO_2 Electrodes in Li-CO_2 Batteries. Energy Environ. Sci. *11*, 1318–1325.
22. Li, X., Wang, H., Chen, Z., Xu, H.-S., Yu, W., Liu, C., Wang, X., Zhang, K., Xie, K., and Loh, K.P. (2019). Covalent-Organic-Framework-Based Li-CO_2 Batteries. Adv. Mater. *31*, e1905879.
23. Huang, S., Chen, D., Meng, C., Wang, S., Ren, S., Han, D., Xiao, M., Sun, L., and Meng, Y. (2019). CO_2 Nanoenrichment and Nanoconfinement in Cage of Imine Covalent Organic Frameworks for High-Performance CO_2 Cathodes in Li-CO_2 Batteries. Small *15*, e1904830.
24. Luo, Z., Liu, L., Ning, J., Lei, K., Lu, Y., Li, F., and Chen, J. (2018). A Microporous Covalent-Organic Framework with Abundant Accessible Carbonyl Groups for Lithium-Ion Batteries. Angew. Chem. Int. Ed. Engl. *57*, 9443–9446.
25. Sun, T., Xie, J., Guo, W., Li, D.-S., and Zhang, Q. (2020). Covalent-Organic Frameworks: Advanced Organic Electrode Materials for Rechargeable Batteries. Adv. Energy Mater. *10*, 1904199.
26. Wang, S., Wang, Q., Shao, P., Han, Y., Gao, X., Ma, L., Yuan, S., Ma, X., Zhou, J., Feng, X., and Wang, B. (2017). Exfoliation of Covalent Organic Frameworks into Few-Layer Redox-Active Nanosheets as Cathode Materials for Lithium-Ion Batteries. J. Am. Chem. Soc. *139*, 4258–4261.
27. Liu, W., Li, X., Wang, C., Pan, H., Liu, W., Wang, K., Zeng, Q., Wang, R., and Jiang, J. (2019). A Scalable General Synthetic Approach toward Ultrathin Imine-Linked Two-Dimensional Covalent Organic Framework Nanosheets for Photocatalytic CO_2 Reduction. J. Am. Chem. Soc. *141*, 17431–17440.
28. Zhu, H.-J., Lu, M., Wang, Y.-R., Yao, S.-J., Zhang, M., Kan, Y.-H., Liu, J., Chen, Y., Li, S.-L., and Lan, Y.-Q. (2020). Efficient electron transmission in covalent organic framework nanosheets for highly active electrocatalytic carbon dioxide reduction. Nat. Commun. *11*, 497.
29. Lu, M., Li, Q., Liu, J., Zhang, F.-M., Zhang, L., Wang, J.-L., Kang, Z.-H., and Lan, Y.-Q. (2019). Installing Earth-Abundant Metal Active Centers to Covalent Organic Frameworks for Efficient Heterogeneous Photocatalytic CO_2 Reduction. Appl. Catal. B *254*, 624–633.
30. Ma, W., Lu, S., Lei, X., Liu, X., and Ding, Y. (2018). Porous Mn_2O_3 Cathode for Highly Durable Li-CO_2 Batteries. J. Mater. Chem. A Mater. Energy Sustain. *6*, 20829–20835.
31. Li, S., Liu, Y., Zhou, J., Hong, S., Dong, Y., Wang, J., Gao, X., Oi, P., Han, Y., and Wang, B. (2019). Monodispersed MnO Nanoparticles in Graphene-an Interconnected N-Doped 3D Carbon Framework as a Highly Efficient Gas Cathode in Li-CO_2 Batteries. Energy Environ. Sci. *12*, 1046–1054.
32. Ge, B., Sun, Y., Guo, J., Yan, X., Fernandez, C., and Peng, Q. (2019). A Co-Doped MnO_2 Catalyst for Li-CO_2 Batteries with Low Overpotential and Ultrahigh Cyclability. Small *15*, e1902220.
33. Liu, L., Zhang, L., Wang, K., Wu, H., Mao, H., Li, L., Sun, Z., Lu, S., Zhang, D., Yu, W., and Ding, S. (2020). Understanding the Dual-Phase Synergy Mechanism in Mn_2O_3-Mn_3O_4 Catalyst for Efficient Li-CO_2 Batteries. ACS Appl. Mater. Interfaces *12*, 33846–33854.
34. Yin, W., Grimaud, A., Azcarate, I., Yang, C., and Tarascon, J.-M. (2018). Electrochemical Reduction of CO_2 Mediated by Quinone Derivatives: Implication for Li-CO_2 Battery. J. Phys. Chem. C *122*, 6546–6554.
35. Ahmadiparidari, A., Warburton, R.E., Majidi, L., Asadi, M., Chamaani, A., Jokisaari, J.R., Rastegar, S., Hemmat, Z., Sayahpour, B., Assary, R.S., et al. (2019). A Long-Cycle-Life Lithium-CO_2 Battery with Carbon Neutrality. Adv. Mater. *31*, e1902518.
36. Mao, Y., Tang, C., Tang, Z., Xie, J., Chen, Z., Tu, J., Cao, G., and Zhao, X. (2019). Long-life Li-CO_2 cells with Ultrafine IrO_2-decorated Few-layered δ-MnO_2 Enabling Amorphous Li_2CO_3 Growth. Energy Storage Mater. *18*, 405–413.
37. Chen, X., Li, Y., Wang, L., Xu, Y., Nie, A., Li, Q., Wu, F., Sun, W., Zhang, X., Vajtai, R., et al. (2019). High-Lithium-Affinity Chemically Exfoliated 2D Covalent Organic Frameworks. Adv. Mater. *31*, e1901640.
38. Wang, D., Wang, K., Sun, L., Wu, H., Wang, J., Zhao, Y., Yan, L., Luo, Y., Jiang, K., Li, Q., et al. (2018). MnO_2 Nanoparticles Anchored on Carbon Nanotubes with Hybrid Supercapacitor-battery Behavior for Ultrafast Lithium Storage. Carbon *139*, 145–155.
39. Kandambeth, S., Mallick, A., Lukose, B., Mane, M.V., Heine, T., and Banerjee, R. (2012). Construction of crystalline 2D covalent organic frameworks with remarkable chemical (acid/base) stability via a combined reversible and irreversible route. J. Am. Chem. Soc. *134*, 19524–19527.
40. Xu, S.-M., Ren, Z.-C., Liu, X., Liang, X., Wang, K.-X., and Chen, J.-S. (2018). Carbonate decomposition: Low-overpotential Li-CO_2 Battery Based on Interlayer-confined Monodisperse Catalyst. Energy Storage Mater. *15*, 291–298.
41. Frisch, M.J., Trucks, G.W., Schlegel, H.B., Scuseria, G.E., Robb, M.A., Cheeseman, J.R., Scalmani, G., Barone, V., Mennucci, B., Petersson, G.A., et al. (2013). Gaussian 09, Revision E.01 (Gaussian).